Chemical surface ageing in ambient conditions of an Al–Fe–Cr approximant phase

2007 J. Phys.: Condens. Matter 19 376207

(http://iopscience.iop.org/0953-8984/19/37/376207)

IOP PUBLISHING JOURNAL OF PHYSICS: CONDENSED MATTER

J. Phys.: Condens. Matter **19** (2007) 376207 (15pp) doi:10.1088/0953-8984/19/37/376207

Chemical surface ageing in ambient conditions of an Al–Fe–Cr approximant phase

D Veys[1], P Weisbecker[1,4], B Domenichini[2], S Weber[3], V Fournée[1,5] and J M Dubois[1]

[1] Laboratoire de Science et Génie des Matériaux et de Métallurgie, UMR 7584 CNRS-INPL-UHP, Ecole des Mines de Nancy, Parc de Saurupt, F-54042 Nancy Cedex, France
[2] Institut Carnot de Bourgogne, UMR 5209 CNRS-Université de Bourgogne, Sciences Mirande, 9 Avenue Alain Savary, F-21078 Dijon Cedex, France
[3] Laboratoire de Physique des Matériaux, UMR 7556 CNRS-INPL-UHP, Ecole des Mines de Nancy, Parc de Saurupt, F-54042 Nancy Cedex, France

E-mail: fournee@lsg2m.org

Received 27 June 2007, in final form 25 July 2007
Published 22 August 2007
Online at stacks.iop.org/JPhysCM/19/376207

Abstract

The γ-$Al_{65}Cr_{27}Fe_8$ phase is a complex metallic alloy with interesting electrochemical properties. Here we present a detailed study of the surface ageing of this alloy when exposed to ambient conditions for a long time. A combination of x-ray reflectivity, photoemission spectroscopy and secondary neutral mass spectroscopy measurements is used to provide a model of the modification of the surface structure and its composition as functions of ageing time. The near surface structure is described by the stacking of three layers. The first layer on top of the substrate corresponds to a mixed metal oxide and is amorphous. The intermediate layer consists of pure aluminum oxy-hydroxide while the outermost layer corresponds to carbonated contaminations. The total thickness of this near-surface region evolves with ageing time, reaching a stable state only after several days.

1. Introduction

Quasicrystals were disclosed in the literature in 1984 by Shechtman *et al* [1] and are typically binary, ternary or quaternary intermetallic compounds, often containing 60–70 atomic per cent of aluminum. This new class of materials has unusual crystallographic structure. Long-range order without translation periodicity is observed together with rotational symmetries that

[4] Present address: Laboratoire des Composites Thermostructuraux, UMR 5801, CNRS-SNECMA-CEA-UB1, 3 Allée de la Boétie, F-33600 PESSAC, France.
[5] Author to whom any correspondence should be addressed.

are forbidden by classical laws of crystallography (for example fivefold axis or tenfold axis). Quasicrystals usually form for specific chemical compositions. Surrounding this small spot in the phase diagram, one often finds crystalline phases with atomic structure very similar to that of the quasicrystalline phase. These periodic crystals are called approximant phases. The unit cell of approximants can be very large, often containing several hundreds of atoms and a local atomic order similar to that found in quasicrystalline phases. Interesting physical properties can result from this structural complexity, which potentially make them useful for a number of technological applications. Quasicrystalline materials would be used in the form of coatings or thin films [2–4]. This allows circumventing their inherent brittleness and taking advantage of their very interesting surface properties such as low surface energy, low friction coefficient and good resistance to oxidation and corrosion [5].

Aluminum being the major component, knowledge of the native oxidized surface on pure Al is a prerequisite for a comprehensive understanding of oxidation occurring by exposure to ambient atmosphere of the surface of quasicrystalline alloys and other complex Al-based crystals. We provide below a short summary of the literature on this subject.

It is well known that aluminum is always covered by a thin protective oxidized film that forms instantaneously in contact with air. The chemistry of such an overlayer has been characterized extensively in the past using a variety of techniques, including x-ray photoemission spectroscopy (XPS), vibrational spectroscopies (IR and Raman) [6] or secondary ion mass spectroscopy (SIMS) [7]. Actually, slight modifications of the chemistry occur in the topmost layers on a much larger time scale for continued air exposure and this 'surface ageing' can affect some properties like wetting. Surface ageing of aluminum was recently studied by Alexander *et al* using XPS [8, 9]. They proposed that the air exposed aluminum surface actually consists of the stacking of three different layers, whose thickness evolves with time. Going from the bulk to the surface, one first finds an amorphous alumina layer with constant thickness, then a second layer containing amorphous aluminum oxy-hydroxides and finally a topmost layer identified as a contamination layer with high C content. The two topmost layers thicken with ageing time. This detailed description of the surface of pure Al is actually quite recent, which is surprising regarding the technological importance of this metal.

Investigations of the air oxidized surfaces of Al-based quasicrystalline and approximant phases were reported in several occasions for different systems. It was found that the thin native oxide layer is mainly composed of alumina [10–14]. In the Al–Cr–Fe system, special attention was paid to the role of chromium [15]. It was shown that chromium also oxidizes under humid conditions and the experiments suggest that the chromium oxide develops below the aluminum oxide layer, forming a double barrier against further oxidation.

Here we extend these studies and focus on the surface ageing of the γ-$Al_{65}Cr_{27}Fe_8$ phase. This complex metallic alloy has a γ-brass structure and is isostructural to cubic Al_9Cr_4 (lattice parameters $a = 9.4$ Å), which can be considered as an approximant of both icosahedral and decagonal quasicrystalline alloys [16, 17]. In this paper, we provide evidence that the air exposed surface can be described by the stacking of three different layers whose thickness and structure evolve upon ageing. Several characterization techniques have been used, including x-ray reflectivity, XPS, angle-resolved photoemission spectroscopy (ARXPS) and secondary neutral mass spectroscopy.

2. Experimental details

Polycrystalline samples were prepared by solid state sintering. First, high purity elements were melted in a water-cooled copper crucible in an induction furnace under a helium atmosphere to

obtain an ingot whose nominal composition was $Al_{65}Cr_{27}Fe_8$. Then the ingot was reduced into powders with particle size in the range 25–50 μm. A solid bulk sample (20–30 mm in diameter) was produced by sintering the powders at high temperature (about 1080 °C) in a carbon matrix under an axial pressure (14 MPa) and in helium atmosphere. The sample surfaces were prepared by mechanical polishing using SiC paper in water lubricant (from 320 grit down to 4000 grit) followed by diamond paste (from 6 μm down to $\frac{1}{4}$ μm) and cleaned with acetone and methanol in an ultrasonic tank. This process leads to a surface presenting mirror-like appearance. Experiments were then performed either directly after polishing or after ageing in ambient conditions for different times (up to 15 days). The relative humidity of the atmosphere ranged from 54% to 67% and the samples were protected from dust.

X-ray specular intensities were collected on an INEL CPS 120 diffractometer equipped with a germanium crystal monochromator. An anode with a Co ($\lambda = 1.788\,97$ Å) target served as the source. A freshly polished sample was mounted on the diffractometer and its position was carefully adjusted. The height of the sample was adjusted so as to reduce by 50% the intensity of the direct beam and the parallelism of the sample with the direct beam was ensured by rotating the sample about its axis and monitoring the intensity of the direct beam. Then, the grazing incidence angle α was varied between 0° and 4°, with a step of 0.01° or 0.02°. For each angle, the specular reflection peak was recorded and integrated with an acquisition time ranging from 30 s to 15 min, depending on the counting rate (which was directly related to the incidence angle α). The front slits were chosen such that the sample intercepted the whole beam before the critical angle α_c. For low angles, the beam was attenuated with an iron foil in order to avoid saturation of the detector. The maximum counting rate allowed by the detector was 5000 cts s^{-1} and the range of reflectivity measured was 10^{-6}, thus it was not possible to collect the whole pattern with one set of operating conditions. The results were gathered on a curve that represents x-ray reflectivity (the ratio between the measured specular intensity and the maximum specular intensity reached) versus Qc ($Qc = 4\pi \sin\alpha/\lambda$). The sample stayed on the diffractometer for 15 days and the measurements were repeated regularly during this period of time. Moreover the temperature of the x-ray room was controlled and regulated so that there was no change of ageing conditions. Modelling of the experimental x-ray reflectivity signal was performed using the software Reflex [18].

Elemental depth profiles were measured by secondary ion mass spectrometry (VG SIMS-Lab), using a scanned Ar^+ ion primary beam (8 keV, 300 nA), detecting simultaneously one metallic ion ($^{27}Al^+$, $^{52}Cr^+$ or $^{56}Fe^+$) and $^{16}O^+$ with a quadrupole mass spectrometer.

XPS surface analysis was performed using a VG Microtech CLAM 4 MCD spectrometer employing a Mg Kα (1253.6 eV) x-ray source operated at 15 kV and 150 W. Typical operating pressures were approximately 1×10^{-7} Pa. Survey (wide-scan) spectra were obtained with a pass energy of 100 eV. Multiplex (narrow-scan) spectra were obtained with a pass energy of 10 eV for C 1s and O 1s lines and a pass energy of 20 eV for Al 2p, Cr 2p and Fe 2p lines. The take-off angle was generally 30° (measured with respect to the surface of the sample). However, one set of angle ARXPS experiments was performed using variable angle XPS in which the take-off angle was varied from 10° to 90°. In this case, only Al 2p and Cr 2p were acquired with a 50 eV pass energy. Data analysis was carried out using CASA XPS software package. In most of the cases, integrated Shirley backgrounds were employed [19] and the peaks were fitted using a 30% mix of Gaussian and Lorentzian line shapes. However, a Shirley background was found inappropriate in the case of the Cr 2p lines and a linear background was employed instead. In addition, an asymmetry parameter was introduced to fit the Cr 2p and Fe 2p lines to account for the asymmetric tail of these metallic components line shapes. The inelastic mean free path of the photoelectrons were calculated assuming an oxide layer [20, 21] and are 15 Å for O 1s and Cr 2p and 26 Å for Al 2p and Cr 3s levels.

3. Results and discussion

3.1. Reflectivity

The oscillations of the x-ray reflectivity signal are due to interference effects of the incident beam resulting from the presence of a film (or different stacked layers) with different material constants on a substrate. The characteristics of these oscillations depend on several parameters [22], as sketched in figure 1. The x-ray reflectivity signal is calculated for a model system consisting of a thin crystallized alumina film on a pure aluminum substrate, a situation close to our experimental system. Figure 1(a) shows that thicker films results in larger periods of the oscillations. Figure 1(b) compares x-ray reflectivity signals obtained from an alumina film and an aluminum oxy-hydroxide film (whose electronic density is closer to that of pure aluminum): small differences in the electronic densities of the film and substrate results in a fast signal decrease with Qc. Roughness at the interfaces introduced in figure 1(c) as a fit parameter affects directly the magnitude of the oscillations. When two layers are stacked on the substrate as shown in figure 1(d), the x-ray reflectivity signal is non-periodic. These different parameters must be taken into account during the fitting of the experimental curves.

Figure 2(a) shows the x-ray reflectivity signal collected on a freshly polished surface and after ageing under ambient atmosphere for 300 h. Experiments show that the signal actually slowly evolves—from curve A to curve B—indicating that the surface slowly evolves as well, reaching a stable state only after several days. The x-ray reflectivity can be simulated theoretically, starting from a model of the surface including the number of layers stacked on the substrate, their thickness, their electronic density and the roughness of the interfaces. We first point out that if only one homogeneous layer was stacked on the substrate, oscillations of the curves would be periodic, in contradiction with experiment. Therefore at least two layers must be taken into account. The initial parameters for the oxidized layer are chosen based on the literature for Al [8, 9] and the electronic density of the substrate is constraint to be that of γ-$Al_{65}Cr_{27}Fe_8$. The best fit obtained assuming either two or three layers stacked on the substrate are shown in figures 2(b) and (c), respectively. It shows that a minimum of *three* different layers must be taken into account in order to obtain a good fit of the experimental data. Table 1 gives the refined parameters of the three layers for various ageing times. Note that the number of electrons per atom relevant to calculate the electronic density parameter is just the atomic number of the elements. Error bars are not calculated by the software, but can be estimated approximately by varying manually the various parameters and observing their influence on the refinement quality. Estimated errors are 0.01 e^- $Å^{-3}$ for the electronic density, 1 Å for the roughness, 2 Å for the thickness of the topmost layer and 0.5 Å for the thickness of the other layers.

Table 2 provides a list of several aluminum and chromium oxides, hydroxides and oxy-hydroxides and their calculated electronic densities. These values may be compared to the experimental ones in order to make some hypothesis on the constitution of each layer stacked over the metal. The outermost surface layer has a very low electronic density and may correspond to a thin contamination layer, similar to what is known for pure aluminum [8, 9]. The thickness of the first layer, directly on top of the substrate, is small and constant with ageing time. Its electronic density is higher than that of the substrate and seems to increase with ageing. The electronic density of the second layer is close to that of the substrate. Its thickness increases with ageing time.

3.2. SNMS

SNMS analyses were performed on both a freshly polished sample and a sample aged for 15 days (about 300 h). The results are shown in figure 3. Depth profiles are plotted as

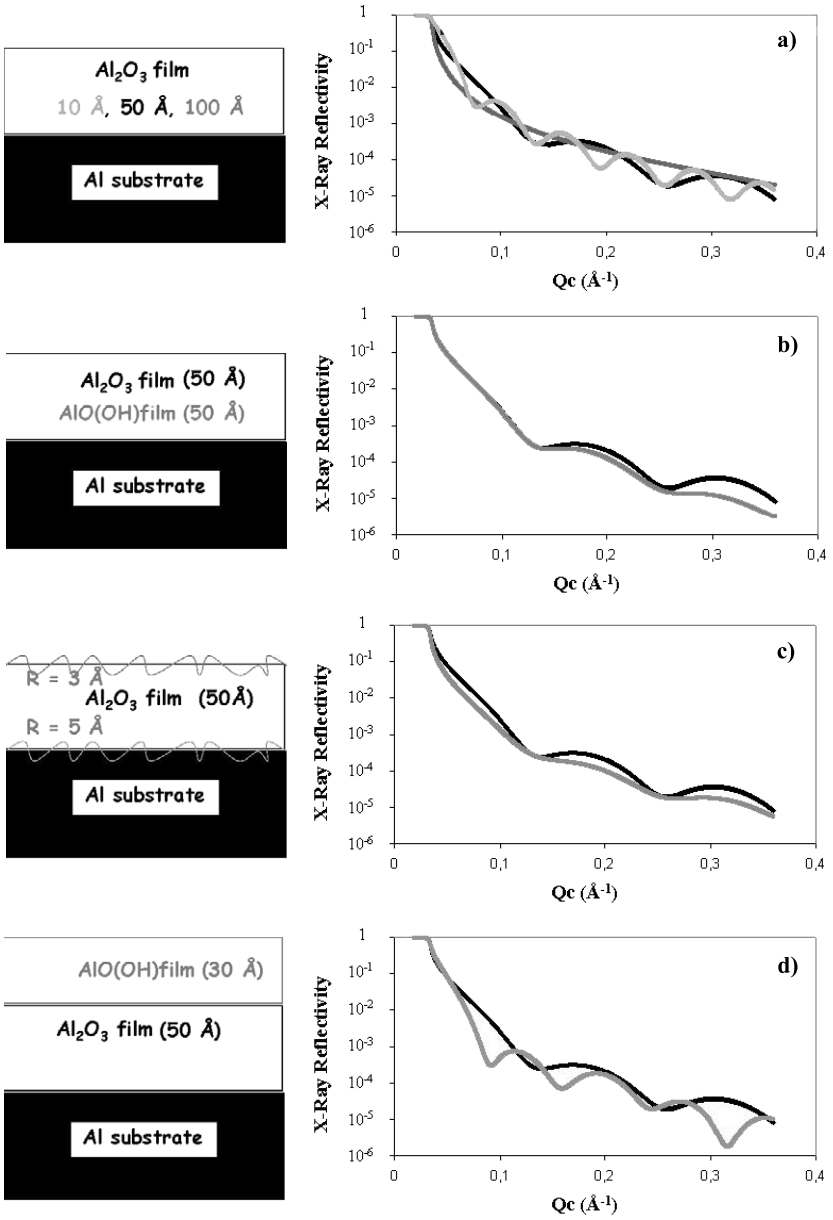

Figure 1. Simulations of x-ray reflectivity versus *Qc* for an oxidized film on an aluminum substrate. The black curves on each graph correspond to a homogeneous crystallized 50 Å thick alumina film with smooth interfaces taken as a reference system. Modifications of this reference system are introduced in (a), (b), (c) and (d) to illustrate the influence of several parameters on x-ray reflectivity line shapes (in grey): (a) influence of the thickness of the film; (b) influence of the electronic density of the film (AlO(OH) film has a lower electronic density than Al_2O_3); (c) influence of interface roughness (roughness amplitudes are 3 Å at the film/air interface and 5 Å at the film/substrate interface); (d) influence of the number of surface layers stacked on the substrate: one overlayer (black curve), two stacked overlayers (grey curve).

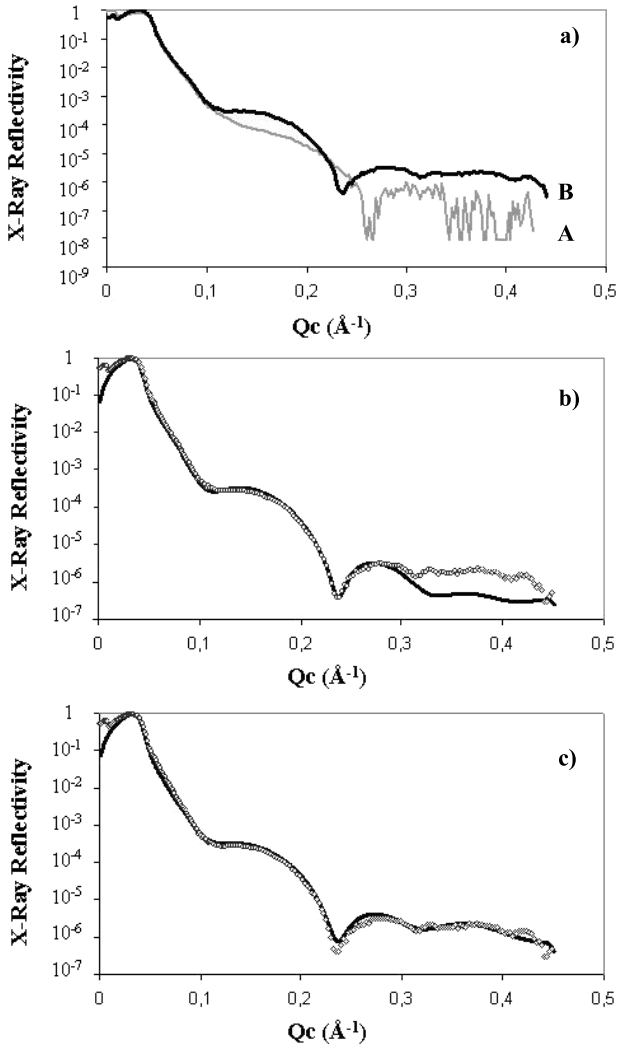

Figure 2. (a) X-ray reflectivity versus Qc measured for the $Al_{65}Cr_{27}Fe_8$ sample on a freshly polished surface (A: grey) and after ageing for 300 h (B: black). ((b), (c)) Fit of the x-ray reflectivity signal of the surface aged for 300 h (empty circles: experimental signal; black curves: calculated signal) using a two-layer model (b) or a three-layer model (c).

a function of sputtering time, where 100 s roughly correspond to a depth of 10 nm. The depth profiles measured for chromium and iron in figures 3(a) and (b), respectively, are very similar. Going from surface to bulk, we first find a region containing almost no chromium nor iron (no signal detected); then an intermediate region where a linear increase of the signal is observed; and finally a plateau where constant values corresponding to the bulk composition are reached. We note that the onset of the signal is shifted towards higher sputtering times upon ageing, indicating that the thickness of the outermost surface layer containing no transition metal increases. This is confirmed in figure 3(d) by oxygen depth profiles. An outermost surface layer with high oxygen content is followed by an inner layer associated with a linear decrease of the intensity. The onset of this linear decrease is also shifted upon ageing. This

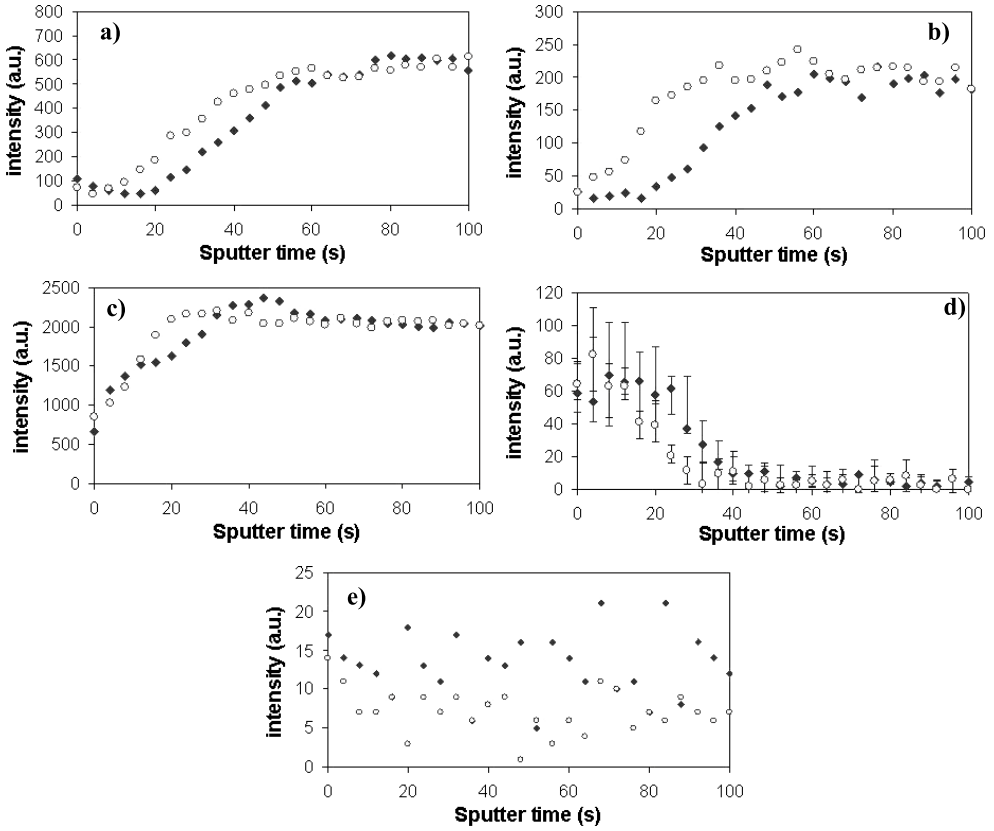

Figure 3. SNMS depth profiles recorded on the surface of an $Al_{65}Cr_{27}Fe_8$ alloy using Ar^+ primary ions (8 keV, 300 nA). Empty circles correspond to a freshly polished surface and black circles to a surface aged for 15 days. (a) $^{52}Cr^+$ measured simultaneously with $^{16}O^+$; (b) $^{56}Fe^+$ measured simultaneously with $^{16}O^+$; (c) $^{27}Al^+$ measured simultaneously with $^{16}O^+$; (d) $^{16}O^+$ measured separately with each one of the other elements; (e) $^{12}C^+$ measured simultaneously with $^{16}O^+$. A sputtering time of 100 s corresponds approximately to a depth of 10 nm.

outermost surface region is also Al rich as pointed out by the Al depth profile in figure 3(c) that should thus correspond to an oxidized layer thickening with ageing time. The carbon content is hardly measured with this experimental set-up (figure 3(e)) and therefore an possible carbon contamination layer may not be detected.

3.3. XPS

The main core level lines (Al 2p, Cr 2p, Fe 2p and O 1s) were recorded as a function of ageing time of the surface. We also performed angle-resolved XPS on either a freshly polished surface or a surface exposed to air for 15 days in order to reveal some details about elemental depth profiles, thickness and uniformity of the oxidized region.

3.3.1. Al 2p, Cr 2p, Fe 2p and O 1s core levels. Figure 4 shows the different core level lines recorded for an aged surface at a take-off angle of 30°. The spectra are fitted according to the method described above. The binding energies (BE), the full width at half-maximum (FWHM) and relative proportions of each component as deduced from these fits are collected in table 3.

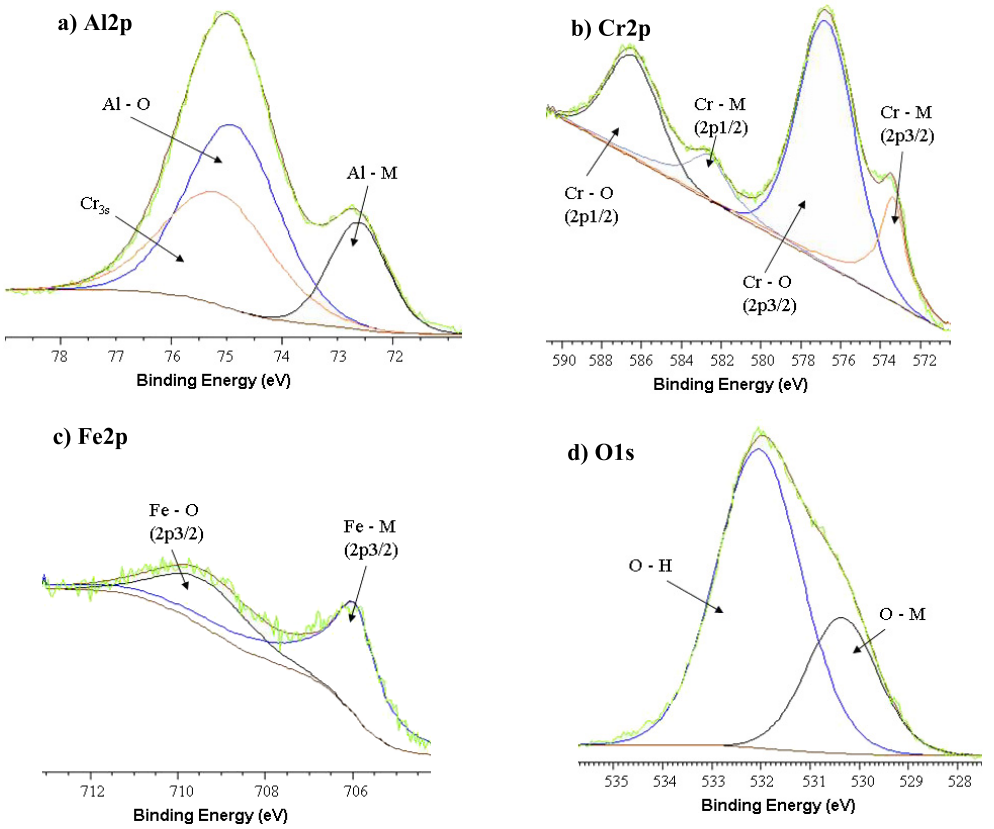

Figure 4. XPS core level lines and their fit acquired on the surface of $Al_{65}Cr_{27}Fe_8$ after ageing for 15 days. (a) Al 2p; (b) Cr 2p; (c) Fe 2p; (d) O 1s. All spectra were recorded at a take-off angle of 30° relative to the surface plane.

(This figure is in colour only in the electronic version)

The O 1s core level (figure 4(d)) is clearly well fitted by two components. The low BE peak can be attributed to an oxide component (O–M) [36, 37] whereas the peak at higher BE can be considered as a hydroxide component (M–OH) [38, 39] (the C 1s core level containing mostly adventitious carbon, an eventual contamination component C–O can be neglected). The Cr 2p (figure 4(b)) and Fe 2p (figure 4(c)) core levels also contain two components: a metallic one (Cr–M [40] and Fe–M [38]) and an oxide one (Cr–O [39] and Fe–O [38]).

Al 2p core level contains also a metallic component (Al–M) [38] and an oxide component (Al–O) [41, 42]. However, the Cr 3s core level also appears in the same energy range: Cr(3s)–M line is located at 74.4 eV whereas the Cr(3s)–O line occurs at 75.1 eV [43]. Because these two components are broad and close in energy, we have taken into account only one global Cr 3s component. The intensity of this component is very low and its area cannot be estimated directly through decomposition of the global Cr 3s/Al 2p peak. However, a good estimation of the area of the Cr 3s line can be obtained through the total area of the Cr $2p_{3/2}$ line according to the relation:

$$A_{\mathrm{Cr3s}} = A_{\mathrm{Cr2p_{3/2}}} \frac{\sigma_{\mathrm{Cr3s}}\lambda_{\mathrm{Cr3s}}}{\sigma_{\mathrm{Cr2p_{3/2}}}\lambda_{\mathrm{Cr2p_{3/2}}}} \tag{1}$$

where A_{Cr3s} and $A_{\mathrm{Cr2p_{3/2}}}$ are the areas of Cr 3s and Cr $2p_{3/2}$ lines, respectively, σ_{Cr3s} and $\sigma_{\mathrm{Cr2p_{3/2}}}$

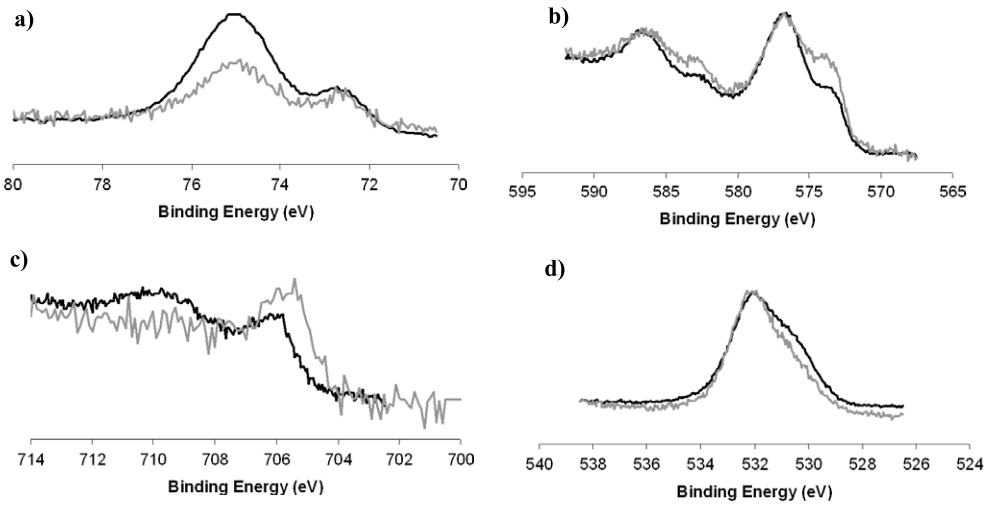

Figure 5. XPS core level lines recorded at a take-off angle of 30° on a freshly polished (grey lines) and after ageing for 15 days (black lines) $Al_{65}Cr_{27}Fe_8$ sample: (a) Al 2p; (b) Cr 2p; (c) Fe 2p; (d) O 1s.

Table 1. Refined electronic density (ρ), thickness (t) and interface roughness (R) deduced from the fit of the x-ray reflectivity signal measured for various ageing times. All the values were obtained using three different surface layers excepted in the last column in which only two surface layers were taken into account.

		1 h	5 h	19 h	22 h	25 h	66 h	138 h	148 h	164 h	265 h	300 h	300 h[a]
3rd layer	R (Å)	3.5	3.5	3.5	3.5	3.5	3	1.8	1.8	1.8	1.8	1.8	
	ρ (e^- Å^{-1})	0.48	0.48	0.48	0.48	0.48	0.48	0.48	0.48	0.48	0.48	0.48	
	t (Å)	8.8	8.8	8.8	8.8	8.8	8.8	10	10.5	10.5	10.5	10.5	
2nd layer	R (Å)	4.2	4.2	4.2	4.2	4.2	3.5	1.6	1.6	1.6	1.6	1.6	6.0
	ρ (e^- Å^{-1})	1.08	1.08	1.08	1.08	1.08	1.08	1.03	1.03	1.03	1.03	1.03	1.03
	t (Å)	31.5	31.1	32	32	32	33	33.5	34	34.5	35.5	36.3	38.0
1st layer	R (Å)	0.5	0.5	0.5	0.5	0.5	0.5	0.5	0.5	0.5	0.5	0.5	1.9
	ρ (e^- Å^{-1})	1.19	1.21	1.25	1.25	1.25	1.25	1.25	1.25	1.25	1.28	1.29	1.28
	t (Å)	14	14	14	14	14	14	14	14	14	14	14	19.7
Substrate	R (Å)	1.5	1.5	1.5	1.5	1.5	1.5	1.5	1.5	1.5	1.5	1.5	1.0
	ρ (e^- Å^{-1})	1.11	1.11	1.11	1.11	1.11	1.11	1.11	1.11	1.11	1.11	1.11	1.11

[a] Corresponds to an adjustment with a two-stacked-layer model (cf figure 3(a)).

are the photoionization cross sections and λ_{Cr3s} and $\lambda_{Cr2p_{3/2}}$ are the corresponding inelastic mean free paths. Then, the position of Al–M (about 72.5 eV [38]) and the FWHM of Al–O (1.9 eV [41, 42]) are fixed and the position of the Cr 3s component is manually adjusted in order to obtain the best possible fit of the Al 2p curve.

Figure 5 shows the spectra acquired for a freshly polished surface and for the same sample exposed to ambient conditions for 15 days. The area under the Al 2p line increases upon ageing (figure 5(a)), due to the growth of the oxide peak, while the metallic component is constant. The relative intensity of the chromium oxide peak also increases with ageing time (figure 5(b)) but the total chromium content detected is lower for the aged sample. The Fe oxide peak is absent just after polishing (figure 5(c)) and grows upon ageing, whereas the intensity of the

Table 2. List of oxides, oxy-hydroxides and hydroxides of Al and Cr and their electronic density calculated from atomic structure and number of electrons per atom (the number of electrons per atom relevant in this case is just the atomic number of the elements).

Formula	Type	Name	ρ (e^- $Å^{-3}$)	Source
α-Al_2O_3	Oxide	Corindon	1.19	[23]
$(Al_2O_3)_5(H_2O)$	Hydrated oxide		1.10	[24]
AlO(OH)	Oxy-hydroxide	Diaspore	1.02	[25]
AlO(OH)	Oxy-hydroxide	Boehmite	0.93	[26]
$Al(OH)_3$	Hydroxide	Bayerite	0.77	[27]
$Al(OH)_3$	Hydroxide	Nordstrandite	0.75	[28]
$Al(OH)_3$	Hydroxide	Gibbsite	0.75	[29]
Cr_3O	Oxide		1.71	[30]
Cr_2O_3	Oxide		1.50	[31]
CrO_2	Oxide		1.40	[32]
CrO_3	Oxide		0.82	[33]
α-CrO(OH)	Oxy-hydroxide	Grimaldiite	1.20	[34]
β-CrO(OH)	Oxy-hydroxide	Gyanaite	1.33	[35]

Table 3. Binding energies (BE), full width at half-maximum (FWHM) and ratio (%) of the different components of the XPS lines shown in figure 4.

	B.E. (eV)	FWHM (eV)	Ratio (%)
Al–M	72.6	1.2	17.7
Al–O	74.9	1.9	48.1
Cr 3s	75.2	2.3	34.2
Cr–M ($2p_{3/2}$)	573.4	1.5	19.6
Cr–O ($2p_{3/2}$)	576.7	3.4	47.0
Cr–M ($2p_{1/2}$)	582.6	2.4	9.8
Cr–O ($2p_{1/2}$)	586.5	3.1	23.5
Fe–M ($2p_{3/2}$)	706.0	1.2	74.5
Fe–O ($2p_{3/2}$)	709.4	2.5	25.5
O–M	530.5	1.7	27.8
O–H	532.0	2.0	72.2

metallic peak decreases. However, the oxide component remains very weak even for the aged sample. Therefore, iron will not be taken into account in the determination of the oxide layer thickness. The evolution of the O 1s line upon ageing is small (figure 5(d)) and a slight increase of the oxide contribution is observed.

3.3.2. Thickness of the oxidized layer. The thickness of the total oxidized layer, containing an oxide part and an oxy-hydroxide part, can be estimated from the area ratio of the oxide and metallic components recorded at different take-off angles.

Assuming a uniform oxide overlayer of thickness t on a metal substrate, the intensity ratio (I_o/I_m) between the oxide and metallic components in the XPS lines may be related to the take-off angle θ by [44–46]:

$$(I_o/I_m) = (D_o\lambda_o/D_m\lambda_m)[1 - \exp[-(t/\lambda_o \sin\theta)]]/\exp[-(t/\lambda_o \sin\theta)] \qquad (2)$$

where D_o and D_m are the atomic densities of metal atoms in the oxide and in the underlying metal substrate, respectively, λ_o and λ_m are the corresponding inelastic mean free paths of emitted electrons and θ is the take-off angle.

Table 4. Thickness of the oxide layer (t), covering rate (γ) and relative mean deviation (rmd) deduced from adjustment by the least square procedure of the experimental data using Strohmeier model [44–46] and Fadley model [47].

		Al			Cr		
		t (Å)	γ	rmd (%)	t (Å)	γ	rmd (%)
Strohmeier model	Polished	9.8	—	83	3.8	—	57
	Aged	11.4	—	62	5.5	—	68
Fadley model	Polished	25.9	0.87	72	6.5	0.87	41
	Aged	42.0	0.87	35	20.7	0.87	23

However, a surface coverage parameter γ is sometimes introduced in order to take into account the non-uniformity of the oxide layer (non-uniform inelastic mean free paths, non-uniform atomic densities). In this case, equation (2) becomes [47]:

$$(I_o/I_m) = (D_o\lambda_o/D_m\lambda_m)(\gamma[1 - \exp[-(t/\lambda_o \sin\theta)]])/([1 - \gamma] + \gamma \exp[-(t/\lambda_o \sin\theta)]). \quad (3)$$

The values of the photoelectron inelastic mean free paths in the oxidized region are calculated using the hypothesis that this oxidized region can be approximated by a crystallized alumina ($\lambda_{oCr} = 15$ Å and $\lambda_{oAl} = 26$ Å) [42, 43]. In the bulk metal, these values become $\lambda_{mCr} = 16$ Å and $\lambda_{mAl} = 24$ Å [42, 43]. Atomic densities of Al and Cr in the $Al_{65}Cr_{27}Fe_8$ alloy are those provided by Demange *et al* [48]: $D_{mAl} = 0.0442$ at.$_{Al}$ Å^{-3} and $D_{mCr} = 0.0184$ at.$_{Cr}$ Å^{-3}. Atomic densities in the oxide layer are more difficult to estimate because the composition and the structure of this oxide are not known. For a crystallized aluminum oxide layer, the Al density would be $D'_{oAl} = 0.043$ at.$_{Al}$ Å^{-3} [49]. In our case, we assume that the oxide layer contains identical amounts of Al and Cr atoms and therefore $D_{oAl} = D_{oCr} \approx 0.02$ at.$_{Al}$ Å^{-3}. Considering these uncertainties on the atomic densities and inelastic mean free paths, we will argue in a first approximation that the ratio $(D_o\lambda_o/D_m\lambda_m)$ in our system is 1 for Al and 0.5 for Cr. Then equations (2) and (3) become respectively (4) and (5) for the aluminum element and (4′) and (5′) for the chromium element.

$$(I_o/I_m) = [1 - \exp[-(t/\lambda_o \sin\theta)]]/\exp[-(t/\lambda_o \sin\theta)] \quad (4)$$

$$(I_o/I_m) = (\gamma[1 - \exp[-(t/\lambda_o \sin\theta)]])/([1 - \gamma] + \gamma \exp[-(t/\lambda_o \sin\theta)]) \quad (5)$$

$$(I_o/I_m) = 0.5[1 - \exp[-(t/\lambda_o \sin\theta)]]/\exp[-(t/\lambda_o \sin\theta)] \quad (4')$$

$$(I_o/I_m) = 0.5(\gamma[1 - \exp[-(t/\lambda_o \sin\theta)]])/([1 - \gamma] + \gamma \exp[-(t/\lambda_o \sin\theta)]). \quad (5')$$

In the following, equations (4) and (4′) will be referred to as the Strohmeier model (uniform oxide layer) and equations (5) and (5′) as the Fadley model (non-uniform oxide layer).

Intensities of the oxide and metal components are deduced from fits of the XPS spectra for each take-off angle using line shape parameters provided in table 3. The results are shown for Al and Cr elements in the case of an aged surface in figures 6(a) and (b), respectively (full squares). Both Strohmeier and Fadley models have been used to fit the variation of (I_o/I_m) as a function of θ by a least square procedure. For the Strohmeier model, the thickness of the oxide layer is the only free parameter of the refinement. For the Fadley model, both the thickness and the surface coverage are free parameters. The (I_o/I_m) values calculated according to these two models are compared to experimental ones in figure 6 and parameters deduced from fit are listed in table 4.

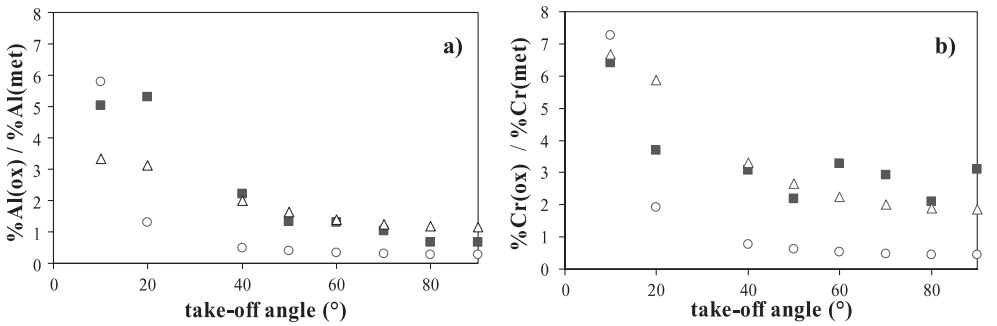

Figure 6. Ratio between oxide and metallic components versus take-off angle for a surface aged for 15 days: (a) Al 2p core level, (b) Cr $2p_{3/2}$ core level. Black squares correspond to experimental data, empty circles correspond to fitted data using Strohmeier model [44–46], empty triangles correspond to fitted data using Fadley model [47].

The Strohmeier model has been used to calculate the thickness of oxide layers on pure aluminum [8, 9], aluminum-based alloys [50], or even stainless steel [51]. But recent studies found that the thickness calculated from Stohmeier model is underestimated [9]. In our case also, the Fadley model provides a better fit of the experimental results and the thicknesses deduced from the fit are two to four times higher than those given by the Strohmeier model. Despite the approximations inherent to these models, the oxide thicknesses listed in table 4 are in good agreement with SNMS and x-ray reflectivity measurements. The conclusions are that the oxide layer gets thicker with increasing ageing time and that the thickness of the oxide calculated from the Fadley model for Al 2p is consistent with values found previously, i.e. about 40 Å. However, the thickness of the oxide layer calculated from the Cr 2p level seems too small. This could confirm that the extreme surface is Cr depleted and that Cr oxide is essentially buried below the Al hydroxide layer directly on top of the substrate.

3.3.3. Thickness of the hydroxide layer. Simmons and Beard [52] have described the oxide film (with a thickness t as described above) grown at the surface of metallic materials as a stacking of three layers. Going from the bulk to the surface, one first finds an oxide layer (thickness t_{MO}), then a hydroxylated layer (thickness t_{hydrox}) and finally a top layer of chemisorbed water (thickness t_{H_2O}). A carbon contamination layer covers this oxide film. In this part, we will focus on the hydroxylated layer.

McCafferty and Wightman have proposed a method to estimate the density of the OH groups at the surface of a metal, based on the deconvolution of O 1s line [53]. The density of OH groups is given by:

$$n_{OH} = \frac{D_O}{0.357} \times \frac{[1 - \exp(-d/\lambda_0 \sin\theta)](I_{OH}/I_{O^{2-}})}{[1 - \exp(-t_{hydrox}/\lambda_0 \sin\theta)][1 + (I_{OH}/I_{O^{2-}})]} \tag{6}$$

where n_{OH} is the density of OH groups at the surface ($Å^{-2}$), D_O is the density of O atoms in the oxide film ($Å^{-3}$), t and t_{hydrox} are respectively the total thickness of the oxide film and the thickness of the hydroxylated layer, λ_o is the inelastic mean free path of O 1s photoelectrons in the oxide film, θ is the take-off angle and $(I_{OH}/I_{O^{2-}})$ is the ratio between the hydroxide and oxide component in the O 1s line.

Equation (6) can be rearranged according to

$$\frac{I_{OH}}{I_{O^{2-}}} = \frac{n_{OH}[1 - \exp(-t_{hydrox}/\lambda_0 \sin\theta)]}{\left[\frac{D_O}{0.357}(1 - \exp(-d/\lambda_0 \sin\theta)) - n_{OH}(1 - \exp(-t_{hydrox}/\lambda_0 \sin\theta))\right]}. \tag{7}$$

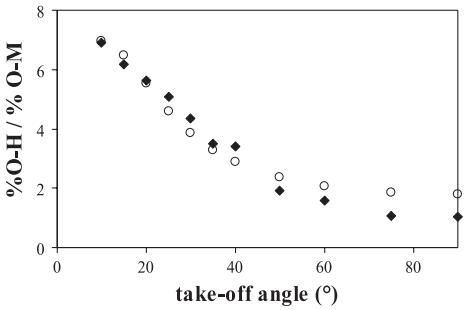

Figure 7. Ratio between O–H and O–M components of O 1s line as a function of take-off angle for a surface aged for 15 days. Black squares correspond to experimental data, empty circles correspond to fit data using McCafferty model [53].

Table 5. Surface densities of OH groups (n_{OH}), thickness of the oxy-hydroxide layer (t_{hydrox}) and relative mean deviation (rmd) deduced from adjustment by the least square procedure of the experimental data using McCafferty model [53].

	n_{OH} (Å^{-2})	t_{hydrox} (Å)	rmd (%)
Freshly polished	0.16	13.9	23
Aged 15 days	0.16	17.5	23

Then, we propose to estimate simultaneously the thickness of the hydroxylated layer t_{hydrox} and the density of OH groups at the surface by a least mean square procedure, using our experimental fits of O 1s lines as a function of take-off angle. The fixed parameters of equation (7) are $D_O = 0.065$ at.Å^{-3} (average value between crystallized Al oxide 0.069 at.Å^{-3} and Cr oxide 0.062 at.Å^{-3} [53]), $\lambda_o = 15$ Å and t is the thickness of the oxide film estimated in the previous section using Fadley model.

The ratios ($I_{OH}/I_{O^{2-}}$) determined from the fit of the experimental spectra for the aged surface are plotted in figure 7 as a function of the take-off angle. Calculated ratios ($I_{OH}/I_{O^{2-}}$) using equation (7) are also shown and fitting parameters t_{hydrox} and n_{OH} are listed in table 5. The quality of the fit using this model is quite good. Furthermore, the density of OH groups at the surface of the $Al_{65}Cr_{27}Fe_8$ sample compares well with values given by McCafferty and Wightman for pure aluminum ($n_{OH} \approx 0.15$ OH.Å^{-2}) and chromium ($n_{OH} \approx 0.13$ OH.Å^{-2}) [53]. Absolute values of the thickness of the hydroxide layer deduced from XPS analysis are lower than those deduced from x-ray reflectivity. This discrepancy may come from an overestimation of the total contribution of the oxide component to O 1s peak (the C–O contribution to O 1s peak being not taken into account) and from the uncertainties about the inelastic mean free paths and atomic densities. However, both techniques converge regarding the trend in the thickening of the hydroxide layer upon ageing.

3.4. Surface model of $Al_{65}Cr_{27}Fe_8$

A surface model valid for pure Al was used as a starting point and we have adjusted this model to the case of our $Al_{65}Cr_{27}Fe_8$ sample by combining all the results described previously. Figure 8 summarizes these results. The surface structure consists in a stacking of three different layers. The first one, directly on top of the substrate, is a mixed amorphous oxide layer of Al, Cr and Fe of constant thickness. The second layer is an oxidized layer, containing only Al and

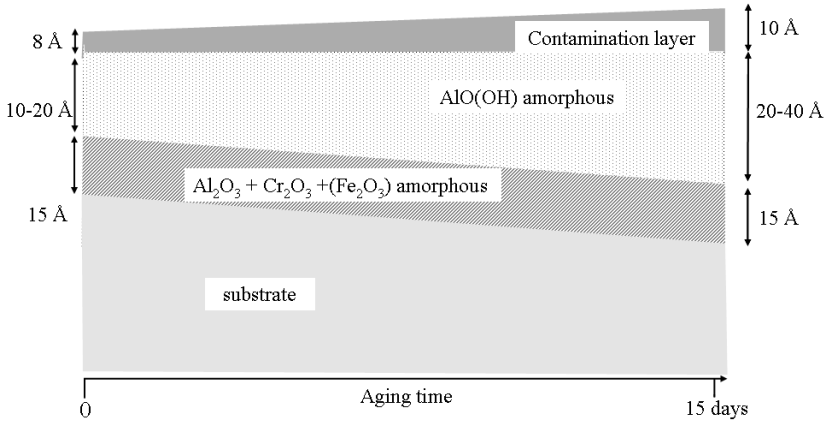

Figure 8. Structure model of the surface of the $Al_{65}Cr_{27}Fe_8$ alloy and its modification upon ageing in ambient atmosphere.

oxygen. This oxy-hydroxide of Al is most likely amorphous and its thickness increases upon ageing time over a period of several weeks. The third layer is the usual contamination layer.

4. Conclusion

By combining three different surface techniques, we managed to propose a consistent detailed model of the native oxidized surface on an Al–Cr–Fe approximant phase. Reflectivity experiments revealed a three-stacked-layer structure; the thickness and electronic density of each layer could be estimated. SNMS results confirmed the multilayer structure and gave some information about the elementary composition of each region of the oxide film. Angle-resolved XPS was used as an alternative way to estimate the thickness of the total oxidized film thickness and the thickness of the hydroxylated layer.

We pointed out the time evolution of thickness and composition of the oxidized layer when then sample is subjected to ageing for weeks in ambient atmosphere.

Acknowledgments

Financial support by the MRT-ERT Quasicristaux Industriels is gratefully acknowledged. We would also like to thank Patricia Thiel and Sylvie Bourgeois for very useful discussions.

References

[1] Shechtman D, Blech I, Gratias D and Cahn J W 1984 *Phys. Rev. Lett.* **53** 1951
[2] Dubois J M, Kang S S and Massiani Y 1993 *J. Non-Cryst. Solids* **153/154** 443
[3] Dubois J M, Kang S S and Perrot A 1994 *Mater. Sci. Eng.* A **179/180** 122
[4] Dubois J M 1997 *New Horizons in Quasicrystals* ed A I Goldman, D J Sordelet, P A Thiel and J M Dubois (Singapore: World Scientific) p 208
[5] Dubois J M 1993 *Phys. Scr.* T **49A** 17
[6] Phambu N 2003 *Mater. Lett.* **57** 2907
[7] Sondag A H M, Raas M C and VanValzen P N T 1989 *Chem. Phys. Lett.* **155** 503
[8] Alexander M R, Thompson G E and Beamson G 2000 *Surf. Interface Anal.* **29** 468
[9] Alexander M R, Thompson G E, Zhou X and Beamson G 2002 *Surf. Interface Anal.* **34** 485
[10] Jenks C J, Chang S L, Anderegg J W, Thiel P A and Lynch D W 1996 *Phys. Rev.* B **54** 9

[11] Pinhero P J, Chang S L, Anderegg J W and Thiel P A 1997 *Phil. Mag.* B **75** 271
[12] Pinhero P J, Sordelet D J, Anderegg J W, Brunet P, Dubois J M and Thiel P A 1999 *Mater. Res. Soc. Symp.* **583** 263
[13] Pinhero P J, Anderegg J W, Sordelet D J, Lograsso T A, Delaney D W and Thiel P A 1999 *J. Mater. Res.* **14** 8
[14] Pinhero P J, Anderegg J W, Sordelet D J, Besser M F and Thiel P A 1999 *Phil. Mag.* B **79** 91
[15] Demange V, Anderegg J W, Ghanbadja J, Machizaud F, Sordelet D J, Besser M, Thiel P A and Dubois J M 2001 *Appl. Surf. Sci.* **173** 327
[16] Demange V, Machizaud F, Dubois J M, Anderegg J W, Thiel P A and Sordelet D J 2002 *J. Alloys Compounds* **342** 24
[17] Demange V, Ghanbaja J, Machizaud F and Dubois J M 2005 *Phil. Mag.* **85** 1261
[18] Gibaud A and Vignaud G 1993 *Acta Crystallogr.* A **49** 642–8
[19] Shirley D A 1972 *Phys. Rev.* B **5** 4709
[20] Tanuma S, Powell C J and Penn D R 1991 *Surf. Interface Anal.* **17** 911
[21] Tanuma S, Powell C J and Penn D R 1993 *Surf. Interface Anal.* **20** 77
[22] Van der Lee A 2000 *Solid State Sci.* **2** 257
[23] Finger L W and Hazen R M 1978 *J. Appl. Phys.* **49** 5823
[24] Yamaguchi G, Okumiya M and Ono S 1969 *Bull. Chem. Soc. Japan* **42** 2247
[25] Busing W R and Levy H A 1958 *Acta Crystallogr.* **11** 798
[26] Christoph G G, Corbato C E, Hofmann D A and Tettenhorst R T 1979 *Clays Clay Miner. Proc. Conf.* **27** 81
[27] Rothbauer R, Zigan F and O'Daniel H 1967 *Z. Kristallogr., Kristallgeom., Kristallphys., Kristallchem.* **125** 317
[28] Bosman H J 1970 *Acta Crystallogr.* B **26** 649
[29] Saalfeld H and Wedde M 1974 *Z. Kristallogr., Kristallgeom., Kristallphys., Kristallchem.* **139** 129
[30] Schoenberg N 1954 *Acta Chem. Scand.* **8** 221
[31] Battle P D, Gibb T C, Nixon S and Harrison W T A 1988 *J. Solid State Chem.* **75** 21
[32] Burdett J K, Miller G J, Richardson J W Jr and Smith J V 1988 *J. Am. Chem. Soc.* **110** 8064
[33] Stephens J S and Cruickshank D W 1970 *Acta Crystallogr.* B **26** 222
[34] Christensen A N, Hansen P and Lehmann M S 1977 *J. Solid State Chem.* **21** 325
[35] Christensen A N, Hansen P and Lehmann M S 1976 *J. Solid State Chem.* **19** 299
[36] Rotole J A and Sherwood P M A 1998 *Surf. Sci. Spectra* **5** 11
[37] Marcus P and Grimal J M 1992 *Corros. Sci.* **33** 805
[38] Barr T L 1978 *J. Phys. Chem.* **82** 1801
[39] Maurice V, Cadot S and Marcus P 2001 *Surf. Sci.* **471** 53
[40] Stypula B and Stoch J 1994 *Corros. Sci.* **36** 2159
[41] Sherwood P 1998 *Surf. Sci. Spectra* **5** 1
[42] Nylund A and Olefjord I 1994 *Surf. Interface Anal.* **21** 283
[43] Allen G C, Tucker P M and Wild R K 1978 *J. Chem. Soc. Faraday Trans.* II **74** 1126
[44] Carlson T A and McGuire G E 1972/73 *J. Electron. Spectrosc. Relat. Phenom.* **1** 161
[45] Carlson T A 1982 *Surf. Interface Anal.* **4** 125
[46] Strohmeier B R 1990 *Surf. Interface Anal.* **15** 51
[47] Fadley C S 1984 *Prog. Surf. Sci.* **16** 275
[48] Demange V 2001 *Thèse de l'Institut National Polytechnique de Lorraine* Nancy
[49] Dong C, Perrot A, Dubois J M and Belin E 1994 *Mater. Sci. Forum* **150/151** 403
[50] Roberts A, Engelberg D, Liu Y, Thompson G E and Alexander M R 2002 *Surf. Interface Anal.* **33** 697
[51] Mantel M and Wightman J P 1994 *Surf. Interface Anal.* **21** 595
[52] Simmons G W and Beard B C 1987 *J. Phys. Chem.* **91** 1143
[53] McCafferty E and Wightman J P 1998 *Surf. Interface Anal.* **26** 549